GEOLOGY | THE GEOLOGICAL SOCIETY OF AMERICA®

https://doi.org/10.1130/G52545.1

Manuscript received 5 July 2024
Revised manuscript received 19 February 2025
Manuscript accepted 2 March 2025

Published online 19 March 2025

Insights into the chemical evolution of sub-arc magmas from the high-pressure electrical conductivity of basaltic and andesitic magmas

Aaron Wolfgang Ashley[1,*], Geeth Manthilake[2], Federica Schiavi[2], and Mainak Mookherjee[1]
[1]Earth Materials Laboratory, Department of Earth, Ocean and Atmospheric Sciences, Florida State University, Tallahassee, Florida 32306, USA
[2]Laboratoire Magmas et Volcans CNRS, IRD, OPGC, Université Clermont Auvergne, 63000 Clermont-Ferrand, France

ABSTRACT

The continental crust is rich in aluminosilicates and formed by the crystallization of arc magmas. However, the magma produced at sub-arc depths is often silica-poor. The chemical evolution of sub-arc magma from silica-poor to aluminosilicate-rich is perplexing. Magnetotelluric (MT) observations in subduction zones and complementary laboratory-based constraints of electrical conductivity (σ) are crucial to understanding this chemical evolution. The σ of a magma is sensitive to pressure (*P*), temperature (*T*), and chemistry (*X*). To date, laboratory-based measurements on the σ of silicate melts have helped to interpret MT observations at $P \leq 2$ GPa. Yet, the melting in subduction zones could occur deeper, at $P \leq 6$–7 GPa. The σ of melt at such pressures is poorly constrained. To address this, we performed experiments at $P \leq 6$ GPa to examine the σ of basaltic to andesitic melts, which are common in subduction zones. We constrained the effects of silica, alumina, alkali, alkaline, and water (H_2O) contents on the σ of melt. The activation volume of σ increases with silica contents. Hence, the σ of basaltic melt is overall greater than that of an andesitic counterpart. The σ of basaltic magma is also less sensitive to *P* than andesitic magma. Water lowers the activation energy and enhances σ for all melt compositions. Our results help constrain how the electrical properties of a magma change with an evolving composition in a subduction zone.

INTRODUCTION

Volcanism along subduction zones helps produce new continental crust, which is broadly andesitic to rhyolitic in composition, i.e., aluminosilicate-rich and ferromagnesian-poor. Yet, the volcanism is promoted by hydrous melting of the mantle wedge (Grove et al., 2012), which tends to create aluminosilicate-poor and ferromagnesian-rich basaltic magma. As the magma ascends, it can become aluminosilicate-rich by assimilation of overlying crustal rock, fractional crystallization, and/or mixing of aluminosilicate-rich and -poor magma endmembers. Andesitic magma may also be produced by slab melting (Yogodzinski et al., 1995) and/or reactive transport processes in the mantle wedge (Hirai et al., 2024). The record of andesitic magma production in subduction zones may be obscured by petrologic and/or geochemical modifications during ascent.

Magnetotelluric (MT) soundings constrain the electrical conductivity (σ) of magmatic regions. The σ is sensitive to the melt chemistry (*X*) and could be used to evaluate an evolving magma composition at depth. The MT measurements are influenced by the σ of the host rock matrix and partially molten pockets or conduits. Laboratory-based constraints on the melt σ as a function of pressure (*P*), temperature (*T*), and *X* are hence crucial for interpreting MT data (Evans, 1999). Previous σ experiments explored a range of silicate melt *X* (Zhang et al., 2021, and references therein). That work has helped to interpret MT measurements of crustal magma chambers at <80 km depth. However, the melting in subduction zones occurs across hundreds of kilometers in distance and depth, based on petrologic (Ducea et al., 2015) and thermal (van Keken et al., 2011) constraints. These depths translate to $P \leq 6$–7 GPa. The σ of silicate melts at such pressures is poorly constrained, which has limited the application of experimental results to interpret MT observations (Unsworth et al., 2023).

To address this issue, we report experimental results on the σ of silicate melts at ≤6 GPa (Text S1 and S2 and Figs. S1–S6 in the Supplemental Material[1]). We investigated the control of *X*, i.e., silica, alumina, alkali, and alkaline contents, on the σ of melts that approximate basaltic to andesitic magmas (Text S1 and S2; Table S1; Figs. S7–S9). Our study extends previous efforts to constrain the combined *P-T-X* effects on the melt σ (Pommier and Le-Trong, 2011) to inform MT observations throughout a subduction zone. Our results should also be helpful to investigate melting in mid-ocean spreading centers, such as the East Pacific Rise (Evans, 1999; Evans et al., 2005; Key et al., 2013; Zhang et al., 2014).

EFFECTS OF *P-T-X* ON ELECTRICAL CONDUCTIVITY

To vary the melt chemistry, we conducted experiments that allowed andesitic melt to react with an MgO-sleeve (Text S1). Yet, the electrical conductivities of these MgO-sleeve experiments are significantly higher than previous measurements on similar melt compositions (Text S2; Fig. S5). The higher σ is not easily explained by minor variations in major oxide chemistry or H_2O contents. Instead, we suspect that the reac-

Aaron Wolfgang Ashley https://orcid.org/0000-0002-5287-5509
*awashley@fsu.edu

[1]Supplemental Material. Supplemental text S1 (methods), S2 (reactive versus non-reactive system), S3 (description of modeling), and S4 (C-O-H volatiles); Figures S1–S10; Tables S1–S4; and references. Please visit https://doi.org/10.1130/GEOL.S.28543616 to access the supplemental material; contact editing@geosociety.org with any questions.

CITATION: Ashley, A.W., et al., 2025, Insights into the chemical evolution of sub-arc magmas from the high-pressure electrical conductivity of basaltic and andesitic magmas: Geology, v. 53, p. 498–502, https://doi.org/10.1130/G52545.1

tion between the melt and MgO also enhanced the σ. This may be due to the concentration gradient of charge-carrying ions, namely Mg and, perhaps, volatiles, from the sleeve into the melt. Compared to a melt at equilibrium, this gradient would provide greater diffusion of ions, which could enhance the transfer of an electrical charge.

To test the effect of the reaction on the measured σ, we also conducted experiments that used relatively non-reactive hexagonal boron nitride (hBN) sleeves (Text S2). The hBN-sleeve experiments show excellent agreement with previous studies and validate our procedure (Fig. S5). Notably, natural magmas also often react with hosting wall rock. Our data suggest that MT surveys should carefully consider the effect of reactive transport on electrical measurements.

The σ from each experiment can be described by an Arrhenius function given by

$$\sigma = \sigma_0 \cdot \exp\left(-\frac{H_a}{RT}\right), \quad (1)$$

where σ_0 is the pre-exponential term (S m^{-1}), H_a is the activation enthalpy (kJ mol^{-1}), R is the ideal gas law (8.314 × 10^{-3} kJ K^{-1} mol^{-1}), and T is the temperature (K) (Table S2; Fig. S3).

The melt σ increases with H_2O contents and decreases with increasing pressure. The basaltic melts are generally more conductive than the andesitic melts (Fig. 1; Figs. S5 and S6; Text S2 and S3). We noted impurities as graphitic flecks in some experiments, but do not find an obvious influence of the carbon on σ, likely due to its isolated occurrence (Text S4). The H_a varies with P and melt chemistry (Table S2). To capture the combined P-T-X effects on σ (Fig. 1; Fig. S4), we expand H_a in Equation 1 as a function of H_2O contents, X, and P, i.e.,

$$H_a\left(X_{H_2O}, X_M, P\right) = E_a\left(X_{H_2O}\right) + PV_a\left(X_M\right), \quad (2)$$

where E_a is the activation energy that varies with the mole fraction of H_2O on an oxide basis (i.e., X_{H2O}) and V_a is the activation volume as a function of X_M (a parameter of the bulk melt chemistry). The activation energy, $E_a(X_{H2O})$, is expanded into

$$E_a\left(X_{H_2O}\right) = E_1 + E_2 \ln\left(1 - X_{H_2O}\right), \quad (3)$$

where E_1 is an activation energy term and E_2 captures the change in E_a with X_{H2O}. The $V_a(X_M)$ can be expanded into

$$V_a\left(X_M\right) = V_1 + V_2 X_M, \quad (4)$$

where V_1 is an activation volume term and V_2 is the dependence of V_a on X_M. We define $X_M = 1 - X_{SiO2}$ where X_{SiO2} is the molar fraction of silica in the melts (Table S2; Fig. 1). At ambient P, silica often forms a polymerized network in the melt by connections between its tetrahedral species, i.e., $[SiO_4]^{-4}$. The dominant mode of conducting electricity in the melts is the diffusion of ions (Kono and Sanloup, 2018). Such ionic diffusivity is impeded by a highly polymerized network. Hence, V_a is greater in relatively polymerized (silica-rich) versus depolymerized (silica-poor) melts (Ni et al., 2015; Zhang et al., 2021).

At ambient P, aluminum often substitutes with silicon as $[AlO_4]^{-5}$. Network-forming tetrahedra may hence be characterized by $TO_4 = [SiO_4]^{-4} + [AlO_4]^{-5}$. Alkali and alkaline oxides may react with and modify the polymer network. The total polymerization in the melt therefore depends on the melt chemistry.

We further examined polymerization in the melts using the molar ratio of non-bridging oxygen ions (NBOs) to TO_4, i.e., X_{NBO}/X_{TO4}. One NBO defines the vertex of a TO_4 that does not connect to another TO_4. Thus, $X_{NBO}/X_{TO4} = 0$ and 4 indicate fully polymerized and depolymerized melts, respectively (Mysen, 1988). We calculated X_{NBO}/X_{TO4} by

$$\frac{X_{NBO}}{X_{TO_4}} = \frac{2\left(\sum X_{MO} + \sum X_{M_2O} - X_{Al_2O_3}\right)}{X_{SiO_2} + 2X_{Al_2O_3}}, \quad (5)$$

where X indicates the molar fraction while the subscripts MO, M_2O, SiO_2, and Al_2O_3 indicate divalent, monovalent, Si, and Al cation oxides, respectively (Table S2; Fig. 1). The addition of H_2O often increases X_{NBO}/X_{TO4} in melts (Ashley et al., 2024, and references therein). The extent of the reaction depends on melt composition, X_{H2O}, T, and P (Stolper, 1982). The X_{NBO}/X_{TO4} of the melts may increase by ≤20% per wt% H_2O (Table S2). The X_{NBO}/X_{TO4} scales with $1 - X_{SiO2}$ and increases as the melts become more basaltic (Fig. S7).

Using $X_M = X_{NBO}/X_{TO4}$ in Equations 2 and 4 produces no significant difference in the calculated σ compared to $X_M = 1 - X_{SiO2}$. The X_{NBO}/X_{TO4} ratio could provide an advantage over $1 - X_{SiO2}$ as it accounts for the roles of other oxides in the melt structure. However, compression increases the coordination of network-forming cations such that $TO_4 \rightarrow TO_5 \rightarrow TO_6$ (Yarger et al., 1995). The X_{NBO}/X_{TO4} estimated from melt chemistry alone does not capture such P effects. Therefore, we use $X_M = 1 - X_{SiO2}$ (Equations 2 and 4) in this study due to its versatility across P.

Regardless of X_M, the modified Arrhenius function highlights the control of chemistry on the effect of P. The V_2 term (dV_a/dX_M) is negative and decreases V_a with increasing X_M (decreasing X_{SiO2}) of the melts (Table 1; Fig. 1). Also, σ is overall enhanced with decreasing X_{SiO2}. Hence, basaltic magmas are generally more conductive and less affected by P than andesitic magmas (Fig. 1).

The addition of H_2O to the melts enhances σ regardless of composition at any explored P or T (Fig. 1). H_2O most strongly enhances σ by lowering E_a. This is likely due to the addition of highly mobile and effective charge-carrying protons.

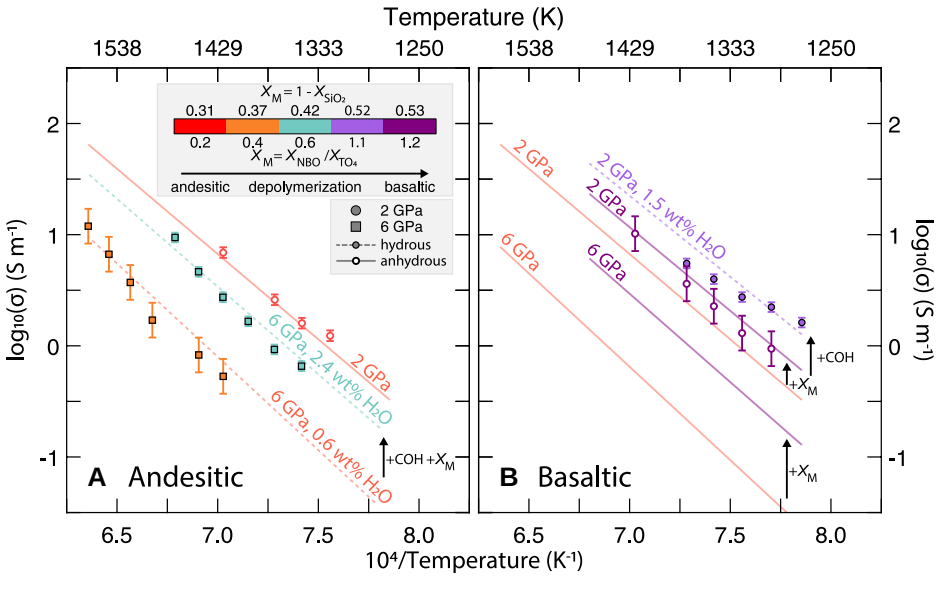

Figure 1. The electrical conductivity (σ) of andesitic (A) and basaltic (B) melts as a function of pressure (*P*), temperature, and volatile contents. Markers display experimental results selected to highlight the *P* and chemistry effects on σ. Lines show predicted σ using the modified Arrhenius function. Solid lines with hollow symbols and dashed lines with solid symbols indicate anhydrous and hydrous melts, respectively. All markers and lines are color-coded to X_M (a parameter of the bulk melt chemistry). The data shown encompass 49–62 wt% SiO_2 (Table S1 [see text footnote 1]). +COH indicates increasing carbon-oxygen-hydrogen volatiles (e.g., H_2O); X_{SiO2} is the molar fraction of silica in the melt; NBO—non-bridging oxygen ions. Error bars show ±1 standard deviation of uncertainty.

TABLE 1. PARAMETERS FOR ELECTRICAL CONDUCTIVITY OF SILICATE MELTS

	Non-reactive*			Reactive*		
	$X_M = X_{NBO}/X_{TO4}$			$X_M = X_{NBO}/X_{TO4}$		
	$X_M = 1 - X_{SiO2}$	No H_2O†	With H_2O§	$X_M = 1 - X_{SiO2}$	No H_2O†	With H_2O§
$\log_{10}(\sigma_0)$ (S m^{-1})	5.7 ± 0.3	5.7 ± 0.3	5.7 ± 0.3	11.6 ± 0.6	11.6 ± 0.6	11.6 ± 0.6
E_1 (kJ mol^{-1})	160 ± 20	160 ± 20	160 ± 20	280 ± 10	280 ± 10	280 ± 10
E_2 (kJ mol^{-1})	–	–	–	170 ± 30	220 ± 30	170 ± 30
V_1 (cm^3 mol^{-1})	17 ± 2	8.1 ± 0.6	8.2 ± 0.7	13 ± 1	8.1 ± 0.6	8.3 ± 0.6
V_2 (cm^3 mol^{-1})	−33 ± 6	−8 ± 2	−8 ± 2	−17 ± 3	−3.8 ± 0.6	−3.8 ± 0.6

Note: Fitting results are separated based on X_M (parameter of the bulk melt chemistry). For this study, we prefer $X_M = 1 - X_{SiO2}$. The X_M values are provided in Table S2 (see text footnote 1) for experiments M1182 to M1193 (Text S2). Uncertainties are at ±1 standard deviation. E_1 is an activation energy term, and E_2 captures the change in E_a with X_{H2O}. V_1 is an activation volume term, and V_2 is the dependence of V_a on X_M.

*Non-reactive and Reactive refer to the experiments that used hexagonal boron nitride (hBN) and MgO sleeves, respectively. The non-reactive parameters assume an approximately constant H_2O content of 0.22 ± 0.07 wt% (Text S2; Table S1).

†The $X_M = X_{NBO}/X_{TO4}$ parameterization does not include H_2O. NBO—non-bridging oxygen ions.

§The $X_M = X_{NBO}/X_{TO4}$ parameterization assumes all available H_2O acts as a network modifying species, i.e., M_2O.

ELECTRIC SIGNALS OF MAGMATIC REGIONS

The total σ observed by MT surveys depends on the σ of silicate melt and crystalline rock, and the connectivity of the melt-rock aggregate. To examine the influence of melt composition, we applied the Hashin-Shtrikman (HS+) model (Hashin and Shtirkman, 1962), which describes the aggregate electrical conductivity (σ_*) as a function of the σ of the melt (σ_m) and matrix (σ_c), and the volume fraction of melt (ϕ), i.e., $\sigma_* = f(\sigma_m, \sigma_c, \phi)$ (Text S3).

We consider the control of basaltic magmas on electrical data from the East Pacific Rise (EPR) mid-ocean spreading center. This setting is ideal to examine low ϕ magmatism at $P \leq$ 2–4 GPa. The σ_* below the EPR is between 0.006 S m^{-1} and ~3 S m^{-1} (Evans, 1999; Evans et al., 2005; Key et al., 2013). At 1523 K, <1 vol% of anhydrous basaltic melt can explain the lower σ_* bound, consistent with earlier estimates of ≤2 vol% melt (Evans et al., 2005) (Fig. 2). The upper σ_* bound requires <20 vol% of anhydrous melt, which agrees well with more recent estimates (Key et al., 2013). Increasing *T* or melt H_2O contents lowers the ϕ needed to explain σ_* (Fig. 2). The σ_c is also enhanced by proton defects (Wang et al., 2006; Karato and Wang, 2013) that could further lower the required ϕ. Yet, the depleted mantle underlying ridge systems typically contains 50–200 ppm H_2O (Peslier et al., 2017). Even a relatively wet mantle underneath the EPR may only explain the lower bound of σ_* (Fig. 2). Channelizing the melt parallel to mantle flow also enhances σ_* (Zhang et al., 2014). Thus, the EPR σ_* likely requires $0 < \phi < 20$ vol% (Fig. 2).

For more silica-rich, andesitic magmas, we apply our constraints to electromagnetic results from the Uturuncu (Bolivia) and Osorno (Chile) volcanoes in the Andes (Fig. 2). For Uturuncu, models from MT data show σ_* from 0.3 S m^{-1} to 3 S m^{-1} (Comeau et al., 2015), which may be produced by 10–20 vol% of hydrous magma (Guo et al., 2017). We find that dissolving 2.4 wt% H_2O in the melt can produce the lower σ_* bound with ~20 vol%, consistent with previous constraints (Guo et al., 2017). Melt inclusion data indicate ≤5.3 wt% H_2O in the magma (Sparks et al., 2008; Muir et al., 2014), which would decrease the ϕ for σ_* by ~80% (Fig. 2). Higher magma H_2O contents (e.g., 10 wt%) and, hence, lower ϕ, may also be possible for the Uturuncu volcano (Laumonier et al., 2017).

For the Osorno volcano, MT work estimated 4–36 vol% of andesitic melt to explain σ_* between 0.025 S m^{-1} and 1.0 S m^{-1} (Díaz et al., 2020). The magma may contain ≤1–2 wt% H_2O based on petrology of the lavas and thermodynamic modeling (Morgado et al., 2019; Bechon et al., 2022). We find that melt with such H_2O contents can explain σ_* with variable ϕ depending on *T* (Fig 2).

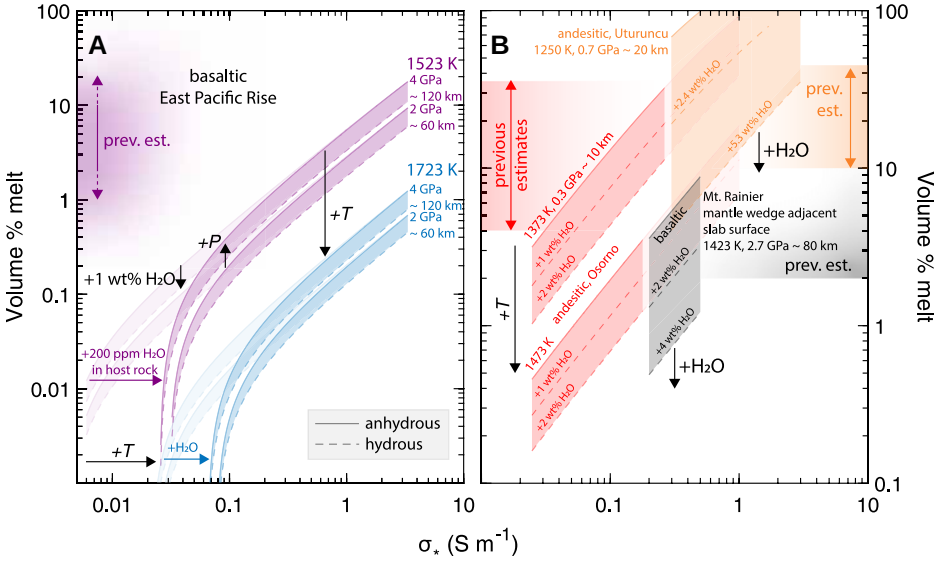

Figure 2. The volume percent of melts (ϕ) required to generate electrical conductivity data from magnetotelluric (MT) measurements (σ_*). (A) Predictions for basaltic magmas in the East Pacific Rise (Evans et al., 2005; Key et al., 2013). The colored faded and non-faded regions show anhydrous and hydrous host rock, respectively. prev. est.—previous estimates. (B) Predictions of subduction zone magmatism. The orange, red, and black lines and shaded regions show results for the Uturuncu volcano (Bolivia; Comeau et al., 2015; Guo et al., 2017) (orange), Osorno volcano (Chile; Díaz et al., 2020) (red), and Mount Rainier (Washington State, USA; McGary et al., 2014) (black) systems. Temperature (*T*), pressure (*P*), and depth conditions are shown for reference. We assume 1 GPa = ~30 km depth. Solid and dashed lines indicate anhydrous and hydrous melts, respectively. We assume anhydrous andesitic and basaltic compositions after our experiments M1182 and M1185 (see Table S1 [see footnote 1]), respectively, and calculated X_M (a parameter of the bulk melt chemistry) = $1 - X_{SiO2}$, and X_{H2O} for various H_2O contents. See Text S3 (see footnote 1) for more details regarding the modeling.

CHEMICAL EVOLUTION OF SUB-ARC MAGMAS

We investigated magmatism in a subduction zone where the melt chemistry may vary between basaltic to andesitic endmembers. We examined a conductor in the mantle wedge beneath Mount Rainier (in the Cascade Range, Washington State, USA) with σ_* between 0.2 S m^{-1} and 0.5 S m^{-1} (McGary et al., 2014). Considering incipient basaltic magmatism in the wedge, we estimate ~3–8 vol% of anhydrous melt could explain σ_* (Fig. 2). Yet, incipient melting is likely to be hydrous with smaller ϕ (McGary et al., 2014). Mafic arc magmas typically contain ~4 wt% H_2O and could become H_2O-saturated during ascent (Plank et al., 2013; Rasmussen et al., 2022). Adding 4 wt% H_2O to the melt lowers the required ϕ to ≤1 vol%, agreeing well with previous ϕ estimates (Fig. 2). We note that these H_2O contents are less than half of prior assessments (McGary et al., 2014). This is perhaps due to an overall enhanced σ by wall-rock reaction (Text S3; Figs. S5 and S6).

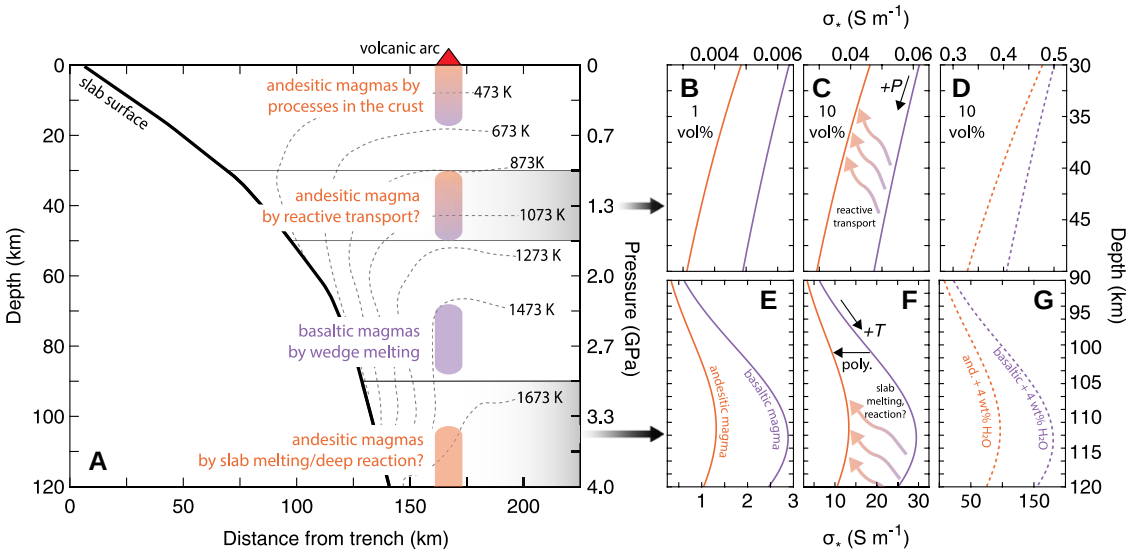

Figure 3. (A) A subduction zone cross section modified from previous work (Syracuse et al., 2010). Dashed lines are isotherms that are shown only in the mantle wedge for clarity. (B–G) Predicted electrical properties (aggregate electrical conductivity, σ*) of magma as a function of volume percent (vol%) and composition. *P*—pressure; *T*—temperature; poly.—polymerization. Panels B–D assume an ascent isotherm of 1273 K for a magma undergoing reactive transport (Hirai et al., 2024). Panels E–G assume the thermal profile in A for deep processes that may yield andesitic magma (Yogodzinski et al., 1995). Panels are arranged by vol% and H_2O contents. The purple and orange lines indicate basaltic and andesitic (and.) compositions, respectively. Solid and dashed lines show σ* for anhydrous and hydrous melts with ~4 wt% H_2O (Plank et al., 2013), respectively. See Text S3 (see footnote 1) for details.

We also note that the H_2O effect on the melt σ increases with *P* (Fig. S5), which could not be previously considered (McGary et al., 2014). Hence, very water-rich (>4 wt% H_2O), incipient melts could produce the σ_* at $\phi < 1$ vol%.

Notably, the Cascadia subduction zone displays a relatively hot geotherm (Syracuse et al. 2010). Geochemical analyses suggest that partial melting of hot subducting slabs could yield andesitic magmas (Yogodzinski et al., 1995). To investigate the potential influence on the ϕ needed to produce σ_*, we predicted the σ_* of andesitic and basaltic melts through a subduction zone (Fig. 3).

At the greatest depths, partial melting of a slab (Yogodzinski et al., 1995) may yield andesitic melt two to three times less conductive than basaltic melt (Fig. 3). Above the slab, we expect melting of the wedge to produce mostly basaltic magmas. Yet, the ascending magma may become andesitic via reactive transport (Hirai et al., 2024). With such chemical evolution, the σ_* may decrease by 10%–50% (Fig. 3). The addition of H_2O to the magma increases the σ_* regardless of melt composition. Regarding the Mount Rainier conductor (Fig. 2), we expect that an increasing ϕ of magma will be needed to explain σ_* if the melt becomes more silica-rich.

Our experimental constraints are useful supplements for MT data to evaluate the chemical evolution of magmas in subduction zones. Additional constraints on the melt volume and H_2O contents from petrologic and geophysical observations could be beneficial for further identifying the melt chemistry at depth.

ACKNOWLEDGMENTS

We thank three anonymous reviewers and the editor, Tracy Rushmer, for their constructive feedback and editorial handling of the manuscript. A.W. Ashley acknowledges support from the Buie, DeVore, and Watkins Fund for the Department of Earth, Ocean and Atmospheric Sciences, Florida State University (Tallahassee, Florida, USA). M. Mookherjee acknowledges the National Science Foundation Award EAR-2246802 and the Global Visitor Fellowship at Earth and Planets Laboratory, Carnegie Institution for Science (Washington, D.C., USA). G. Manthilake acknowledges funding received from the Centre National de la Recherche Scientifique–Institut National des Sciences de l'Univers (CNRS-INSU) PNP program. The multi-anvil apparatus of Laboratoire Magmas et Volcans (Aubière, France) is financially supported by the CNRS (Instrument National de l'INSU). This is ClerVolc contribution No. 688.

REFERENCES CITED

Ashley, A.W., Bajgain, S., and Mookherjee, M., 2024, Mobility of magmas within the Earth: Insights from the elasticity and transport properties of hydrous albitic melts: Geochemistry, Geophysics, Geosystems, v. 25, https://doi.org/10.1029/2024GC011510.

Bechon, T., Billon, M., Namur, O., Bolle, O., Fugmann, P., Foucart, H., Devidal, J.-L., Delmelle, N., and Vander Auwera, L., 2022, Petrology of the magmatic system beneath Osorno volcano (central southern volcanic zone, Chile): Lithos, v. 426–427, https://doi.org/10.1016/j.lithos.2022.106777.

Comeau, M.J., Unsworth, M.J., Ticona, F., and Sunagua, M., 2015, Magnetotelluric images of magma distribution beneath Volcán Uturuncu, Bolivia: Implications for magma dynamics: Geology, v. 43, p. 243–246, https://doi.org/10.1130/G36258.1.

Díaz, D., Zúñiga, F., and Castruccio, A., 2020, The interaction between active crustal faults and volcanism: A case study of the Liquiñe-Ofqui Fault Zone and Osorno volcano, southern Andes, using magnetotellurics: Journal of Volcanology and Geothermal Research, v. 393, https://doi.org/10.1016/j.jvolgeores.2020.106806.

Ducea, M.N., Saleeby, J.B., and Bergantz, G., 2015, The architecture, chemistry, and evolution of continental magmatic arcs: Annual Review of Earth and Planetary Sciences, v. 43, p. 299–331, https://doi.org/10.1146/annurev-earth-060614-105049.

Evans, R.L., 1999, Asymmetric electrical structure in the mantle beneath the East Pacific Rise at 17°S: Science, v. 286, p. 752–756, https://doi.org/10.1126/science.286.5440.752.

Evans, R.L., Hirth, G., Baba, K., Forsyth, D., Chave, A., and Mackie, R., 2005, Geophysical evidence from the MELT area for compositional controls on oceanic plates: Nature, v. 437, p. 249–252, https://doi.org/10.1038/nature04014.

Grove, T.L., Till, C.B., and Krawczynski, M.J., 2012, The role of H_2O in subduction zone magmatism: Annual Review of Earth and Planetary Sciences, v. 40, p. 413–439, https://doi.org/10.1146/annurev-earth-042711-105310.

Guo, X., Li, B., Ni, H., and Mao, Z., 2017, Electrical conductivity of hydrous andesitic melts pertinent to subduction zones: Journal of Geophysical Research: Solid Earth, v. 122, p. 1777–1788, https://doi.org/10.1002/2016JB013524.

Hashin, Z., and Shtrikman, S., 1962, A variational approach to the theory of the effective magnetic permeability of multiphase materials: Journal of Applied Physics, v. 33, p. 3125-3131, https://doi.org/10.1063/1.1728579.

Hirai, Y., Tamura, Y., Hanyu, T., Chang, Q., Timm, C., and Hoernle, K., 2024, Why are oceanic arc basalts Ca-rich and Ni-poor? Insights from olivine-hosted melt inclusions from Kibblewhite Volcano in the Kermadec arc: Chemical Geology, v. 662, https://doi.org/10.1016/j.chemgeo.2024.122218.

Karato, S.I., and Wang, D., 2013, Electrical conductivity of minerals and rocks, *in* Karato, S.I., ed., Physics and Chemistry of the Deep Earth: Chichester, UK, John Wiley & Sons, p. 145–182, https://doi.org/10.1002/9781118529492.ch5.

Key, K., Constable, S., Liu, L., and Pommier, A., 2013, Electrical image of passive mantle upwelling beneath the northern East Pacific Rise: Nature, v. 495, p. 499–502, https://doi.org/10.1038/nature11932.

Kono, Y., and Sanloup, C., eds., 2018, Magmas Under Pressure: Advances in High-Pressure Experiments on Structure and Properties of Melts: Amsterdam, Elsevier, 514 p., https://doi.org/10.1016/C2016-0-01520-6.

Laumonier, M., Gaillard, F., Muir, D., Blundy, J., and Unsworth, M., 2017, Giant magmatic water reservoirs at mid-crustal depth inferred from electrical

conductivity and the growth of the continental crust: Earth and Planetary Science Letters, v. 457, p. 173–180, https://doi.org/10.1016/j.epsl.2016.10.023.

McGary, R.S., Evans, R.L., Wannamaker, P.E., Elsenbeck, J., and Rondenay, S., 2014, Pathway from subducting slab to surface for melt and fluids beneath Mount Rainier: Nature, v. 511, p. 338–340, https://doi.org/10.1038/nature13493.

Morgado, E., Morgan, D.J., Harvey, J., Parada, M.Á., Castruccio, A., Brahm, R., Gutiérrez, F., Georgiev, B., and Hammond, S.J., 2019, Localised heating and intensive magmatic conditions prior to the 22–23 April 2015 Calbuco volcano eruption (Southern Chile): Bulletin of Volcanology, v. 81, https://doi.org/10.1007/s00445-019-1280-2.

Muir, D.D., Blundy, J.D., Hutchinson, M.C., and Rust, A.C., 2014, Petrological imaging of an active pluton beneath Cerro Uturuncu, Bolivia: Contributions to Mineralogy and Petrology, v. 167, https://doi.org/10.1007/s00410-014-0980-z.

Mysen, B.O., 1988, Structures and properties of silicate melts, *in* Marfunin, A.S., ed., Advanced Mineralogy: Berlin, Springer: p. 238–254, https://doi.org/10.1007/978-3-642-78523-8_14.

Ni, H., Hui, H., and Steinle-Neumann, G., 2015, Transport properties of silicate melts: Reviews of Geophysics, v. 53, p. 715–744, https://doi.org/10.1002/2015RG000485.

Peslier, A.H., Schönbächler, M., Busemann, H., and Karato, S.I., 2017, Water in the Earth's interior: Distribution and origin: Space Science Reviews, v. 212, p. 743–810, https://doi.org/10.1007/s11214-017-0387-z.

Plank, T., Kelley, K.A., Zimmer, M.M., Hauri, E.H., and Wallace, P.J., 2013, Why do mafic arc magmas contain ~4 wt% water on average?: Earth and Planetary Science Letters, v. 364, p. 168–179, https://doi.org/10.1016/j.epsl.2012.11.044.

Pommier, A., and Le-Trong, E., 2011, "SIGMELTS": A web portal for electrical conductivity calculations in geosciences: Computers & Geosciences, v. 37, p. 1450–1459, https://doi.org/10.1016/j.cageo.2011.01.002.

Rasmussen, D.J., Plank, T.A., Roman, D.C., and Zimmer, M.M., 2022, Magmatic water content controls the pre-eruptive depth of arc magmas: Science, v. 375, p. 1169–1172, https://doi.org/10.1126/science.abm5174.

Sparks, R.S.J., Folkes, C.B., Humphreys, M.C., Barfod, D.N., Clavero, J., Sunagua, M.C., McNutt, S.R., and Pritchard, M.E., 2008, Uturuncu volcano, Bolivia: Volcanic unrest due to mid-crustal magma intrusion: American Journal of Science, v. 308, p. 727–769, https://doi.org/10.2475/06.2008.01.

Stolper, E., 1982, The speciation of water in silicate melts: Geochimica et Cosmochimica Acta, v. 46, p. 2609–2620, https://doi.org/10.1016/0016-7037(82)90381-7.

Syracuse, E.M., van Keken, P.E., and Abers, G.A., 2010, The global range of subduction zone thermal models: Physics of the Earth and Planetary Interiors, v. 183, p. 73–90, https://doi.org/10.1016/j.pepi.2010.02.004.

Unsworth, M., Comeau, M.J., Diaz, D., Brasse, H., Heit, B., Favetto, A., Pomposiello, C., Barcelona, H., Peri, G., and Ticona, F., 2023, Crustal structure of the Lazufre volcanic complex and the Southern Puna from 3-D inversion of magnetotelluric data: Implications for surface uplift and evidence for melt storage and hydrothermal fluids: Geosphere, v. 19, p. 1210–1230, https://doi.org/10.1130/GES02506.1.

van Keken, P.E., Hacker, B.R., Syracuse, E.M., and Abers, G.A., 2011, Subduction factory: 4. Depth-dependent flux of H_2O from subducting slabs worldwide: Journal of Geophysical Research: Solid Earth, v. 116, B1, https://doi.org/10.1029/2010JB007922.

Wang, D., Mookherjee, M., Xu, Y., and Karato, S.I., 2006, The effect of water on the electrical conductivity of olivine: Nature, v. 443, p. 977–980, https://doi.org/10.1038/nature05256.

Yarger, J.L., Smith, K.H., Nieman, R.A., Diefenbacher, J., Wolf, G.H., Poe, B.T., and McMillan, P.F., 1995, Al coordination changes in high-pressure aluminosilicate liquids: Science, v. 270, p. 1964–1967, https://doi.org/10.1126/science.270.5244.1964.

Yogodzinski, G.M., Kay, R.W., Volynets, O.N., Koloskov, A.V., and Kay, S.M., 1995, Magnesian andesite in the western Aleutian Komandorsky region: Implications for slab melting and processes in the mantle wedge: Geological Society of America Bulletin, v. 107, p. 505–519, https://doi.org/10.1130/0016-7606(1995)107<0505:MAITWA>2.3.CO;2.

Zhang, B., Yoshino, T., Yamazaki, D., Manthilake, G., and Katsura, T., 2014, Electrical conductivity anisotropy in partially molten peridotite under shear deformation: Earth and Planetary Science Letters, v. 405, p. 98–109, https://doi.org/10.1016/j.epsl.2014.08.018.

Zhang, B.H., Guo, X., Yoshino, T., and Xia, Q.K., 2021, Electrical conductivity of melts: Implications for conductivity anomalies in the Earth's mantle: National Science Review, v. 8, https://doi.org/10.1093/nsr/nwab064.

Printed in the USA